

# Study of Spectral Modification of Hadrons through Electromagnetic Probes<sup>a</sup>

**Sourav Sarkar**

*Variable Energy Cyclotron Centre  
1/AF Bidhannagar, Kolkata-700 064*

The medium modification of vector meson properties and its effects on thermal photon and dilepton emission rates from hot/dense hadronic matter are discussed. The role of spectral changes of hadrons in explaining the WA98 photon data and the CERES/NA45 dilepton data with similar initial conditions is demonstrated.

## 1 Introduction

A fundamental property of QCD with two light quark flavours is the approximate chiral symmetry which plays a very important role in the understanding of low energy hadron physics. Since this symmetry is not manifest in the observed particle degeneracies it is believed that chiral symmetry is spontaneously broken by the vacuum. Under conditions of high temperature or density one expects that the QCD vacuum will undergo substantial modifications leading to the restoration of chiral symmetry. The chiral condensate which has a non-trivial value in the broken phase acts as the order parameter of this transition. Though hadron masses can be expressed in terms of various condensates through the QCD sum rules for example, there are uncertainties connected with the approximations used in their evaluation. The change in the condensate in hot/dense environment is expected to show up in the spectral function of the vector mesons. Concomitant to these phenomena, quarks and gluons, which are normally bound within hadrons are expected to undergo a deconfinement transition at sufficiently high temperature or baryon density leading to the formation of quark gluon plasma (QGP)<sup>1</sup>.

Relativistic collisions of heavy ions provide a rich arena for the study of strongly interacting matter under extreme conditions in the laboratory. Data from the Super Proton Synchrotron (SPS) have already been analysed and the first results from the Relativistic Heavy Ion Collider (RHIC) have started to appear. Electromagnetic probes, *viz.*, photons and dileptons have long been recognized as the most direct probes of the collision<sup>2</sup>. Owing to the nature of their interaction they undergo minimal scatterings and are by far the best markers of the entire space-time evolution of the collision. Both photons and dileptons couple to hadrons through spin one ( $J^P = 1^-$ ) mesons. The dilepton spectra in particular, exhibits a resonant structure which, in the low mass regime includes the  $\rho$  and the  $\omega$  mesons. It has been emphasized that the properties of the vector mesons undergo nontrivial medium modifications in a hot and/or dense medium such as likely to be produced in relativistic

<sup>a</sup>Presented at DAE Symposium on Nuclear Physics, Kolkata, India, 26-30 Dec. 2001

nuclear collisions. Consequently the spectral modifications of these vector mesons would be clearly revealed in the invariant mass spectra of the dileptons through the shift of the resonant peaks.

In the following we will discuss the role of medium modification of hadronic properties in explaining the photon and dilepton spectra from heavy ion collisions at the CERN SPS. Let us first consider the data obtained from Pb-Pb collisions at 158 A GeV reported by the WA98 Collaboration<sup>3</sup> which shows the transverse momentum spectra of excess photons above those coming from the decay of  $\pi^0$  and  $\eta$  mesons. These excess photons are believed to arise due to (a) the hard collisions of partons in the colliding nuclei and (b) a thermal medium - QGP or hot/dense hadronic matter. We have seen<sup>4</sup> that the above spectra can be explained using a reasonable set of parameters if the medium effects of the vector meson properties are consistently incorporated in the invariant rates as well as in the equation of state. It is worth recalling that the single photon data for S+Au collisions could also be explained in a similar scenario<sup>5</sup>. However, other attempts to explain the photon spectra without invoking medium effects exist in the literature<sup>6,7,8,9,10</sup>.

Our aim now is to check whether the same scenario can explain the dilepton data obtained in Pb+Au collisions at SPS by the CERES/NA45 Collaboration<sup>11</sup>. The possible sources in the low mass region are the dileptons coming from the decays of hadrons at freeze-out and from the in-medium propagation and decay of vector mesons. The data shows a significant enhancement in the mass region 0.3 to 0.6 GeV which can be explained<sup>12</sup> by a substantial negative shift of the mass of vector mesons (the  $\rho$  meson in particular) in the thermal medium. A large broadening of the  $\rho$  meson spectral function due to scattering off baryons can also explain this enhancement<sup>13</sup>.

In the following we will see that both the WA98 photon spectra as well as the CERES/NA45 dilepton spectra for higher multiplicities can be explained by either of the two scenarios of relativistic nuclear collision<sup>14,4</sup>: (a)  $A + A \rightarrow \text{QGP} \rightarrow \text{Mixed Phase} \rightarrow \text{Hadronic Phase}$  or (b)  $A + A \rightarrow \text{Hadronic Matter}$ ; with downward shift of vector meson masses and initial temperature  $\sim 200$  MeV. The photon yield is seen to be insensitive to the broadening of vector mesons<sup>15</sup>, although the CERES dilepton data admits such a scenario as mentioned above. The effects of the thermal shift of the hadronic spectral functions on both photon and dilepton emission have been considered in Ref.<sup>15</sup> for an exhaustive set of models. An appreciable change in the space-time integrated yield of electromagnetic probes was observed for universal scaling and Quantum Hadrodynamics (QHD) model and we will consider only these in our discussion.

This report is organized as follows. In the following section we will briefly outline the phenomenology of medium effects on the vector mesons in the thermal environment which we have considered. In section 3 we will consider the static photon and dilepton rates due to different processes. Then in section 4 we will describe the dynamics of space-time evolution followed by the results of our calculation in section 5. We will conclude with a summary and discussions in section 6.

## 2 Medium Effects

A substantial amount of literature has been devoted to the issue of temperature and/or density dependence of hadrons within various models<sup>15,16,17,13,18</sup>. In this work we will consider medium modifications of vector mesons in two different scenarios : the universal scaling hypothesis and the Quantum Hadrodynamics (QHD) model.

In the scaling hypothesis, the parametrization of in-medium quantities (denoted by  $*$ ) at finite temperature,  $T$  and baryon density<sup>19</sup>,  $n_B$  is

$$\frac{m_V^*}{m_V} = \frac{f_V^*}{f_V} = \frac{\omega_0^*}{\omega_0} = \left(1 - 0.2 \frac{n_B}{n_B^0}\right) \left(1 - \frac{T^2}{T_c^2}\right)^\lambda, \quad (1)$$

where  $V$  stands for vector mesons,  $f_V$  is the coupling between the electromagnetic current and the vector meson field,  $\omega_0$  is the continuum threshold,  $T_c$  is the critical temperature and  $n_B^0$  is the baryon density of normal nuclear matter. Mass of the nucleon also varies with temperature according to Eq. (1) (pseudo scalar masses remain unchanged). The particular exponent  $\lambda = 1/2$  (1/6) is known as Nambu (Brown-Rho) scaling<sup>17</sup>. We will use  $\lambda = 1/2$  in our calculations. Note that there is no definite reason to believe that all the in-medium dynamical quantities are dictated by a single exponent  $\lambda$ . This is the simplest possible ansatz (see<sup>15</sup> for a discussion). The effective mass of  $a_1$  is estimated by using Weinberg's sum rules<sup>20</sup>.

In the Quantum Hadrodynamics model<sup>21,22</sup> of nuclear matter the vector meson properties are modified due to coupling with nucleonic excitations. The nucleons interact through the exchange of scalar  $\sigma$  and the vector  $\omega$  mesons and their mass is modified due to the scalar condensate. This is evaluated in the Relativistic Hartree Approximation (RHA). Coupling with these modified nucleonic excitations induce changes in the  $\rho$  and  $\omega$  meson masses. This modification is contained in the meson self energy which appears in the Dyson-Schwinger equation for the effective propagator in the medium. The interaction vertices are provided by the Lagrangian

$$\mathcal{L}_{VNN}^{\text{int}} = g_{VNN} \left( \bar{N} \gamma_\mu \tau^a N V_a^\mu - \frac{\kappa_V}{2M_N} \bar{N} \sigma_{\mu\nu} \tau^a N \partial^\nu V_a^\mu \right), \quad (2)$$

where  $V_a^\mu = \{\omega^\mu, \bar{\rho}^\mu\}$ ,  $M_N$  is the free nucleon mass,  $N$  is the nucleon field and  $\tau_a = \{1, \vec{\tau}\}$ ,  $\vec{\tau}$  being the Pauli matrices. The real part of the vector meson self-energy due to  $NN$  polarization is responsible for the mass shift (see<sup>23,24,25,26</sup>). The  $\rho - \pi$  interaction is given by

$$\mathcal{L}_{\rho\pi\pi}^{\text{int}} = -g_{\rho\pi\pi} \rho_\mu^\vec{\tau} \cdot (\vec{\pi} \times \partial^\mu \vec{\pi}) + \frac{1}{2} g_{\rho\pi\pi}^2 (\vec{\pi} \times \vec{\rho}_\mu) \cdot (\vec{\pi} \times \vec{\rho}^\mu). \quad (3)$$

This makes the dominant contribution to the imaginary part of the  $\rho$  self-energy though the pole shift (real part) is negligibly small. We have evaluated the spectral function of  $\rho$  due to its coupling with the pion and nucleons (Eqs. (2) and (3)) in the thermal bath for finite three momentum at non-zero temperature and density.

### 3 Thermal Photon and Dilepton Emission Rates

In this section, we briefly recapitulate the main equations relevant for evaluating photon and dilepton emission from a thermal source. The emission rate of real photons with four momentum  $p_\mu = (E, \vec{p})$  can be expressed in terms of the imaginary part of the retarded electromagnetic current correlation function as<sup>2</sup>

$$E \frac{dR}{d^3p} = -\frac{1}{(2\pi)^3} g^{\mu\nu} \text{Im}W_{\mu\nu}^R(p) f_{BE}(E, T), \quad (4)$$

where

$$W_{\mu\nu}^R(p) \equiv i \int d^4x e^{ip \cdot x} \theta(x_0) \langle [J_\mu^{em}(x), J_\nu^{em}(0)] \rangle_\beta, \quad (5)$$

$J_\mu^{em}$  being the electromagnetic current of quarks or hadrons. All the information about the thermal medium which produces the photons or dileptons resides in the current correlator  $W^{\mu\nu}$ . The lowest order processes contributing to thermal photon emission from quark gluon plasma are the QCD Compton and annihilation processes<sup>27</sup>. It has been shown recently<sup>28</sup> that the two-loop contribution leading to bremsstrahlung and  $q\bar{q}$  annihilation with scattering is of the same order as the lowest order processes. The total rate of emission per unit four-volume at temperature  $T$  is given by

$$E \frac{dR}{d^3p} = \frac{5}{9} \frac{\alpha\alpha_s}{2\pi^2} \exp(-E/T) \left[ \ln\left(\frac{2.912 E}{g^2 T}\right) + 4 \frac{(J_T - J_L)}{\pi^3} \left\{ \ln 2 + \frac{E}{3T} \right\} \right] \quad (6)$$

where  $J_T \simeq 4.45$  and  $J_L \simeq -4.26$ .

Considering the hadronic matter to be made up of  $\pi$ ,  $\rho$ ,  $\omega$ ,  $\eta$  and  $a_1$  mesons, the imaginary part of  $W^{\mu\nu}$  gives the amplitudes of a number of hadronic processes. We have considered the reactions  $\pi\rho \rightarrow \pi\gamma$ ,  $\pi\pi \rightarrow \rho\gamma$ ,  $\pi\pi \rightarrow \eta\gamma$ ,  $\pi\eta \rightarrow \pi\gamma$  and the decays  $\rho \rightarrow \pi\pi\gamma$  and  $\omega \rightarrow \pi\gamma$  with dressed vector propagators to estimate photon emission from hadronic matter.

To obtain the dilepton emission rate, the additional part to be included in Eq. (4) corresponds to the free propagation of the virtual photon and its subsequent decay to lepton pairs. This gives,

$$\frac{dR}{d^4p} = -\frac{\alpha}{12\pi^4 p^2} g^{\mu\nu} \text{Im}W_{\mu\nu}^R(p) \left(1 + \frac{2m_l^2}{p^2}\right) \sqrt{1 - \frac{4m_l^2}{p^2}} f_{BE}(E, T) \quad (7)$$

where  $m_l$  is the lepton mass.

In the QGP, the dominant channel for dilepton productions is quark-antiquark annihilation. The rate for this process is obtained from the lowest order diagram

contributing to the current correlator  $W^{\mu\nu}$  and is obtained as,

$$\frac{dR}{d^4p} = \sum_f e_f^2 \frac{\alpha^2}{4\pi^4} \left(1 + \frac{2m_l^2}{p^2}\right) \sqrt{1 - \frac{4m_l^2}{p^2}} f_{BE}(E, T) \quad (8)$$

Now let us consider dilepton production in the hadronic medium. In order to obtain the rate of dilepton emission from hadronic matter ( $\rho/\omega \rightarrow l^+l^-$ ) from Eq. (7) the electromagnetic current correlator is expressed in terms of the effective propagator of the vector particle in the thermal medium using vector meson dominance (VMD) so as to obtain

$$\begin{aligned} \text{Im}W_{\mu\mu}^R = & \frac{e^2 m_V^4}{g_V^2} \left[ \frac{2\text{Im}\Pi_V^T}{(p^2 - m_V^2 + \text{Re}\Pi_V^T)^2 + (\text{Im}\Pi_V^T)^2} \right] \\ & + \frac{\text{Im}\Pi_V^L}{(p^2 - m_V^2 + \text{Re}\Pi_V^L)^2 + (\text{Im}\Pi_V^L)^2} \end{aligned} \quad (9)$$

where  $\text{Im}\Pi_V^{T(L)}$  is the transverse(longitudinal) part of the retarded self-energy of vector mesons arising out of interaction with excitations in the medium. The dilepton rate from pion annihilation for example, can be obtained from  $\rho$  self-energy due to  $\pi - \pi$  polarisation in the medium. In the approximation  $\Pi_\rho^T = \Pi_\rho^L = \Pi_\rho$  we have

$$\text{Im}W_{\mu\mu}^R = \frac{3e^2 m_\rho^{*4}}{g_{\rho\pi\pi}^2} \left[ \frac{\text{Im}\Pi_\rho}{(M^2 - m_\rho^{*2})^2 + (\text{Im}\Pi_\rho)^2} \right], \quad (10)$$

where  $m_\rho^{*2} = m_\rho^2 - \text{Re}\Pi_\rho$  and  $p^2 = M^2$ , the invariant mass of the lepton pair. This is proportional to the familiar electromagnetic form factor of the pion.

#### 4 Space-Time Evolution

The observed spectrum originating from an expanding hadronic matter is obtained by convoluting the static rates given above with the expansion dynamics. This is done using (3+1) dimensional relativistic hydrodynamics assuming boost invariance in the longitudinal direction and cylindrical symmetry in the transverse plane. The initial energy density and transverse velocity profiles are taken as

$$\epsilon(\tau_i, r) = \frac{\epsilon_0}{e^{(r-R_A)/\delta} + 1}; \quad v_r = v_0 \left( \frac{r}{R_A} \right)^\alpha \quad (11)$$

with  $\alpha = 1$ . The other essential input one requires is the equation of state (EOS) which provides the cooling law. For the QGP sector we use the bag model equation of state with two flavour degrees of freedom. The hadronic phase is taken to consist of  $\pi$ ,  $\rho$ ,  $\omega$ ,  $\eta$  and  $a_1$  mesons and nucleons. The medium effects enter through the effective

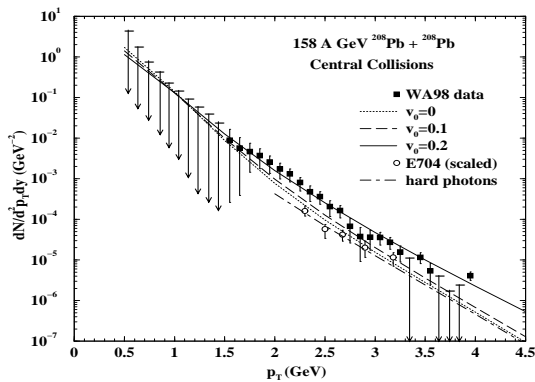


Figure 1: Total photon yield in Pb + Pb collisions at 158 A GeV at CERN-SPS. The system is formed in the QGP phase with initial temperature  $T_i = 190$  MeV.

masses in the expressions for energy density and pressure. The entropy density is then parametrized as,

$$s_H = \frac{\epsilon_H + P_H}{T} \equiv 4a_{\text{eff}}(T) T^3 = 4 \frac{\pi^2}{90} g_{\text{eff}}(m^*, T) T^3 \quad (12)$$

where  $g_{\text{eff}}$  is the effective statistical degeneracy. Thus, we can visualize the finite mass of the hadrons having an effective degeneracy  $g_{\text{eff}}(m^*, T)$ . The velocity of sound which plays a significant role in the expansion, also becomes a function of  $T$  and differs substantially from its value corresponding to an ideal gas ( $1/\sqrt{3}$ ). The initial temperature of the system is obtained by solving the equation

$$T_i^3 = \frac{3.6}{\pi R_A^2 4a_{\text{eff}}(T_i) \tau_i} \frac{dN_\pi}{dy} \quad (13)$$

where  $dN_\pi/dy$  is the total pion multiplicity ( $\sim 1.5 \times$  charge multiplicity),  $R_A$  is the radius of the system,  $\tau_i$  is the initial thermalization time and  $a_{\text{eff}} = (\pi^2/90) g_{\text{eff}}(T_i)$ . When the system is produced in the QGP phase,  $g_{\text{eff}}$  is replaced by  $g_{\text{QGP}}$  which for two quark flavours is 37. If the quark and gluon masses are non-zero in the thermal bath then the effective degeneracy of the QGP,  $g_{\text{QGP}}^{\text{eff}}$ , defined by Eq. (12) can be lower than 37, resulting in a higher value of  $T_i$  for a given multiplicity according to Eq. (13). Note that the change in the expansion dynamics as well as the value of the initial temperature due to medium effects relevant for a hot hadronic gas also enters through the effective statistical degeneracy. The freeze-out temperature  $T_F$  is taken as 120 MeV.

## 5 Results

In Fig. 1, the photon yield with QGP in the initial state is shown for three different values of the initial transverse velocity. The yield from hadronic matter during the

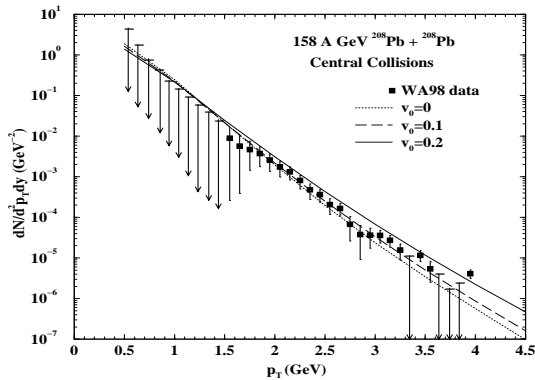


Figure 2: Total photon yield in Pb + Pb collisions at 158 A GeV at CERN SPS. The system is formed in the hadronic phase with the hadronic masses approaching zero at initial temperature  $T_i = 200$  MeV.

mixed and hadronic phases are calculated with medium effects in the scaling scenario. All the three curves represent the sum of the thermal and the prompt photon contribution which includes possible finite  $k_T$  effects of the parton distributions. The later, shown separately by the dot-dashed line also explains the scaled  $pp$  data from E704 experiment<sup>29</sup>. We observe that the photon spectra for the initial velocity profile given by Eq. (11) with  $v_0 = 0.2$  explains the WA98 data reasonably well. It is found that a substantial fraction of the photons come from mixed and hadronic phase. The contribution from the QGP phase is small because of the small life time of the QGP ( $\sim 1$  fm/c).

To check whether the existence of the QGP phase essential to reproduce the WA98 data, we have considered two possibilities: (a) pure hadronic model without medium-modifications, and (b) pure hadronic model with scaling hypothesis according to Eq.(1). In the former case,  $T_i$  is found to be  $\sim 250$  MeV for  $\tau_i = 1$  fm/c and  $dN/dy = 700$ , which appears to be too high for the hadrons to survive. Therefore this possibility should be excluded. On the other hand, the second case with an assumption of  $T_i = T_c$  (which is just for simplicity) leads to  $T_i \sim 200$  MeV, at  $\tau_i = 1$  fm/c, which is not unrealistic. In this case, the hadronic system expands and cools and ultimately freezes out at  $T_f=120$  MeV. The results for three values of the initial radial velocity including the prompt photon contribution are shown in Fig. 2. The experimental data are well reproduced for vanishing initial transverse velocity also. This indicates that a simple hadronic model is inadequate. Either substantial medium modifications of hadrons or the formation of QGP in the initial stages is necessary to reproduce the data. It is rather difficult to distinguish between the two at present.

We will now compare the results of our calculation with the dilepton spectra obtained by the CERES/NA45 Collaboration. We have considered<sup>12</sup> dileptons with transverse momentum  $p_T$  above 200 MeV/c and an opening angle  $\Theta_{ee} > 35$  mrad.

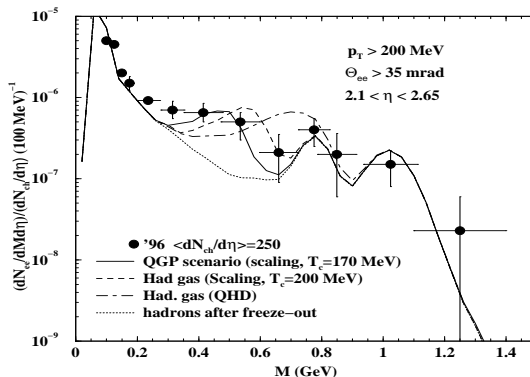


Figure 3: Dilepton spectra for  $\langle N_{ch} \rangle = 250$  for different initial states and mass variation scenarios.

These are kinematical cuts relevant for the CERES detector and are incorporated as described in <sup>30</sup>. In all the figures, the quantity  $\langle N_{ch} \rangle$  indicates the average number of charged particles per unit rapidity interval in the pseudorapidity range  $2.1 < \eta < 2.65$ . In all the cases background due to hadron decays are added to the thermal yields.

We display the results for  $dN_{ch}/d\eta = 250$  in Fig. 3. In this case apart from the hadronic gas scenario we have also considered a deconfined initial state with  $T_i = 180$  MeV which evolves into a hadronic gas via a mixed phase. The observed enhancement of the dilepton yield around  $M \sim 0.3 - 0.6$  GeV can be reproduced with the QGP initial state, once the variation of vector meson masses in the mixed and the hadronic phases are taken into account (solid line). The data is also reproduced by a hadronic initial state with  $T_i = 190$  MeV in the universal mass variation scenario (dashed line). The  $\rho$ -peak in the dilepton spectra shifts towards lower  $M$  for universal scaling compared to QHD model, indicating a strong medium effect in the former case.

The dilepton spectra for QGP and hadronic initial states for  $dN_{ch}/d\eta = 350$  is shown in Fig. 4. Results with hadronic initial state and universal scaling of hadronic masses with temperature describes the data reasonably well. We see that with the temperature dependent mass from QHD model the low mass enhancement of the experimental yield cannot be reproduced. A good description of the data can be obtained by taking  $T_i = 200$  MeV with QGP initial state for  $T_c = 190$  MeV. We also show the results due to large broadening of the  $\rho$  spectral function in the medium. The broadening of  $\rho$  is modelled by assuming the temperature dependent width as :  $\Gamma_\rho(T) = \Gamma_\rho(0)/(1 - T^2/T_c^2)$ .

## 6 Summary and Discussions

We have evaluated the high energy photon yield in Pb + Pb collisions at CERN SPS energies with two different initial conditions. In the first scenario, we start with the assumption of the formation of a QGP phase at an initial temperature of



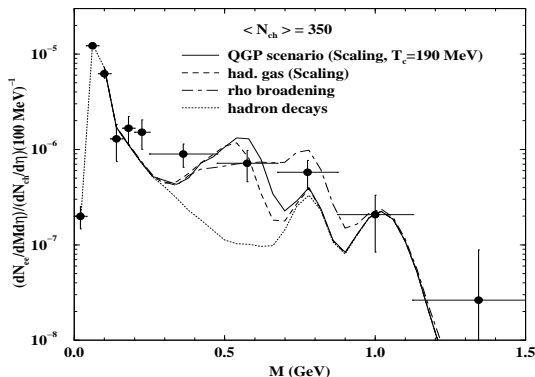


Figure 4: Dilepton spectra for  $\langle N_{ch} \rangle = 350$  for different initial states and mass variation scenarios.

$\sim 200$  MeV and then the system continues through mixed phase and hadronic phase before freeze-out. In the second scenario, we assume a chirally symmetric phase where the hadronic masses approach zero at a temperature  $\sim 200$  MeV and then the system evolves towards freeze-out. The effects of the variation of hadronic masses on the photon yield have been considered both in the cross section as well as in the equation of state. The photon spectra reported by the WA98 collaboration are well reproduced in both cases. We have also studied the dilepton yield measured by CERES experiment for two values of the charge multiplicity in Pb + Au interactions. It is observed that the data can be described by both QGP and hadronic initial states with an initial temperature  $\sim 200$  MeV. We have assumed  $\tau_i = 1$  fm/c at SPS energies, which may be considered as the lower limit of this quantity, because the transit time (the time taken by the nuclei to pass through each other in the CM system) is  $\sim 1$  fm/c at SPS energies and the thermal system is assumed to be formed after this time has elapsed. There are also uncertainties in the value of  $T_c$ <sup>31</sup>, a value of  $T_c \sim 200$  MeV may be considered as an upper limit. Moreover, the photon emission rate from QGP given by Eq. (6), evaluated in Refs.<sup>27,28</sup> by resumming the hard thermal loops is strictly valid for  $g \ll 1$  whereas the value of  $g$  is  $\sim 2$  at  $T \sim 200$  MeV. At present it is not clear whether the rate in Eq. (6) is valid for such a large value of  $g$ .

**Acknowledgement:** The work reported here was done in collaboration with J. Alam, P. Roy, T. Hatsuda, T. K. Nayak and B. Sinha at various stages.

#### References:

1. Proc. of Quark Matter'99, Nucl. Phys. **A 661** (1999).
2. L. McLerran and T. Toimela, Phys. Rev. **D 31**, 545 (1985); C. Gale and J. I. Kapusta, Nucl. Phys. **B357**, 65 (1991); E. V. Shuryak, Phys. Rep. **61**,

- 71 (1980); J. Alam, S. Raha and B. Sinha, Phys. Rep. **273**, 243 (1996); W. Cassing and E. L. Bratkovskaya, Phys. Rep., **308**, 65 (1999).
3. M. M. Aggarwal et al., WA98 Collaboration, Phys. Rev. Lett. **85**, 3595 (2000); nucl-ex/0006007; nucl-ex/0008004.
  4. J. Alam, S. Sarkar, T. Hatsuda, T. K. Nayak and B. Sinha, Phys. Rev. C **63**, 021901R (2001).
  5. S. Sarkar, P. Roy, J. Alam and B. Sinha, Phys. Rev. C **60**, 054907 (1999).
  6. C. Y. Wong and H. Wang, Phys. Rev. C **58**, 376 (1998).
  7. K. Gallmeister, B. Kämpfer and O. P. Pavlenko, Phys. Rev. C **62**, 057901 (2000).
  8. D. Yu. Peressounko and Yu. E. Pokrovsky, hep-ph/0009025.
  9. D. K. Srivastava and B. Sinha, nucl-th/0006018;
  10. P. Huovinen, P. V. Ruuskanen and S. S. Rasanen, nucl-th/0111052.
  11. G. Agakichiev *et al*, CERES Collaboration, Phys. Lett. **B 422**, 405 (1998); B. Lenkeit, Doctoral Thesis, Universitaet Heidelberg (1998).
  12. S. Sarkar, J. Alam and T. Hatsuda, nucl-th/0011032.
  13. R. Rapp and J. Wambach, Adv. Nucl. Phys. **25**, 1 (2000).
  14. J. Alam, P. Roy, S. Sarkar and B. Sinha, nucl-th/0106038.
  15. J. Alam, S. Sarkar, P. Roy, T. Hatsuda and B. Sinha, Ann. Phys. (N.Y.) **286**, 159 (2000).
  16. T. Hatsuda and T. Kunihiro, Phys. Rep. **247**, 221 (1994).
  17. G. E. Brown and M. Rho, Phys. Rep. **269**, 333 (1996).
  18. R. D. Pisarski, hep-ph/9503330.
  19. G. E. Brown, C. M. Ko, Z. G. Wu nad L. H. Xia, Phys. Rev. C **43** 1881 (1991).
  20. S. Weinberg, Phys. Rev. Lett. **18**, 507 (1967).
  21. B. D. Serot and J. D. Walecka, *Advances in Nuclear Physics Vol. 16*, Plenum Press, New York 1986.
  22. S. A. Chin, Ann. Phys. (N.Y.) **108**, 301 (1977).
  23. S. Sarkar, J. Alam, P. Roy, A. K. Dutt-Mazumder, B. Dutta-Roy and B. Sinha, Nucl. Phys. **A634**, 206 (1998).
  24. P. Roy, S. Sarkar, J. Alam and B. Sinha, Nucl. Phys. **A 653** 277 (1999).
  25. C. Song, P. W. Xia and C. M. Ko, Phys. Rev. **C52**, 408 (1995).
  26. T. Hatsuda, H. Shiomi and H. Kuwabara, Prog. Theor. Phys. **95**, 1009 (1996).
  27. J. I. Kapusta, P. Lichard, and D. Seibert, Phys. Rev. **D44**, 2774 (1991); R. Baier, H. Nakkagawa, A. Niegawa and K. Redlich, Z. Phys. **C53**, 433 (1992).
  28. P. Aurenche, F. Gelis, H. Zaraket and R. Kobes, Phys. Rev. **D 58**, 085003 (1998); F. D. Steffen and M. H. Thoma, hep-ph/0103044; D. Dutta et al, hep-ph/0104134.
  29. E704 Collaboration, D. L. Adams et al, Phys. Lett. **B 345**, 569 (1995).
  30. J. Sollfrank, P. Huovinen, M. Kataja, P. V. Ruuskanen, M. Prakash and R. Venugopalan, Phys. Rev. **C55**, 392 (1997).
  31. F. Karsch, Nucl. Phys. (Proc. Suppl.), **B 83**, 14 (2000).